PNAS RESEARCH ARTICLE | IMMUNOLOGY AND INFLAMMATION

Bacterial indole-3-lactic acid affects epithelium–macrophage crosstalk to regulate intestinal homeostasis

Kaiyuan Yu[a], Qianqian Li[a], Xuan Sun[a], Xianping Peng[a], Qiang Tang[a], Hongyu Chu[b], Lu Zhou[b], Bangmao Wang[b], Zhemin Zhou[c], Xueqin Deng[a], Jianming Yang[a], Junqiang Lv[a], Ran Liu[a], Chunhui Miao[a], Wei Zhao[d], Zhi Yao[a,1], and Quan Wang[a,1]

Edited by Chun-jun Guo, Weill Cornell Medicine, New York, NY; received June 3, 2023; accepted September 27, 2023 by Editorial Board Member Carl F. Nathan

Tryptophan and its derivatives perform a variety of biological functions; however, the role and specific mechanism of many tryptophan derivatives in intestinal inflammation remain largely unclear. Here, we identified that an *Escherichia coli* strain (*Ec*-TMU) isolated from the feces of tinidazole-treated individuals, and indole-3-lactic acid (ILA) in its supernatant, decreased the susceptibility of mice to dextran sulfate sodium–induced colitis. *Ec*-TMU and ILA contribute to the relief of colitis by inhibiting the production of epithelial CCL2/7, thereby reducing the accumulation of inflammatory macrophages in vitro and in vivo. Mechanistically, ILA downregulates glycolysis, NF-κB, and HIF signaling pathways via the aryl hydrocarbon receptor, resulting in decreased CCL2/7 production in epithelial cells. Clinical evidence suggests that the fecal ILA level is negatively correlated with the progression indicator of inflammatory bowel diseases. These results demonstrate that ILA has the potential to regulate intestinal homeostasis by modulating epithelium–macrophage interactions.

ILA | intestinal homeostasis | macrophage | CCL2/7 | CCR2

Significance

The microbiome is crucial to the maintenance of intestinal homeostasis. Here, we investigated that an isolated human fecal bacteria strain and its derived ILA regulated intestinal homeostasis. ILA reduces glycolysis, NF-κB, and HIF pathways to decrease CCL2/7 in epithelial cells, thereby decreasing the accumulation of inflammatory macrophages. These findings determine the role and mechanism of bacteria-derived ILA in regulating intestinal homeostasis and provide evidence that ILA has therapeutic potential for IBD.

Several factors contribute to the maintenance of intestinal homeostasis, including the intestinal barrier (1), microbiota (2, 3), and the immune system (3). Microbial dysbiosis and disruption of immune homeostasis lead to many intestinal diseases, including inflammatory bowel diseases (IBD); however, the causal roles between the microbiome and the maintenance of homeostasis remain unclear.

The gut microenvironment includes numerous types of cells, including epithelia, innate immune cells [macrophages, innate lymphoid cells (ILCs)], and adaptive immune cells [T helper (Th)1, 2, 17 and regulatory T (Treg) cells]. The communication between these cells is essential for intestinal homeostasis. Intestinal macrophages require constant replenishment by circulating monocytes throughout adulthood, and targeting macrophage–monocyte differentiation has been suggested to improve intestinal inflammation in IBD patients (4). On the basis of major histocompatibility complex II (MHCII) and Ly6C expression in mice, intestinal macrophages are divided into four subsets, P1 ($Ly6C^{+}MHCII^{-}$), P2 ($Ly6C^{+}MHCII^{+}$), and P3-P4 ($Ly6C^{-}MHCII^{+}$), of which pro-inflammatory P1/P2 cells produce TNF-α, IL-1, and IL-6 in inflammatory states and anti-inflammatory P3-P4 cells produce IL-10 to decrease inflammatory cytokines (5). In addition, macrophages with high CX3CR1 expression also have anti-inflammatory properties (5).

In the composition of the intestinal bacteria, obligatory anaerobic bacteria have a definitive advantage over facultative anaerobes (6). However, certain facultative anaerobes, such as *Lactobacillus gallinarum*, which could inhibit colorectal cancer, are essential for the maintenance of intestinal homeostasis, despite their low percentage in the intestine (7). In addition, we isolated a facultative anaerobic strain from metronidazole-treated mouse feces, with alleviating effects on DSS-induced colitis (8), indicating that certain facultative anaerobes are essential for regulating gut homeostasis.

Tryptophan is metabolized in three ways: host pathways (the kynurenine and serotonin pathways) and microbial pathways (the indole pathways), all of which are crucial for maintaining intestinal homeostasis (9). Indole derivatives [including indoleacetic acid, indole-3-aldehyde (IAld), and indoleacrylic acid (IA)] act as agonists for the aryl hydrocarbon receptor (AHR). AHR is an essential transcription factor that translocates into the nucleus and dimerizes with its partner, the aryl hydrocarbon receptor nuclear translocator (ARNT), to induce transcription of anti-inflammatory target genes (10, 11), such as CYP1A1 and CYP1B1 (12). IAld, produced by bacteria such as *Lactobacilli*, stimulates IL-22 secretion by ILC3 via AHR, thereby enhancing the intestinal barrier function (13). In addition, a study discovered that IA derived from the commensal *P. russellii* could improve goblet cell differentiation and reduce susceptibility to colitis (14). However, the effects and mechanisms of other tryptophan derivatives on the maintenance of intestinal homeostasis remain unexplored.

Author affiliations: [a]Key Laboratory of Immune Microenvironment and Disease (Ministry of Education), Tianjin Institute of Immunology, The Province and Ministry Co-sponsored Collaborative Innovation Center for Medical Epigenetics, Department of Immunology, School of Basic Medical Sciences, Tianjin Medical University, Tianjin 300070, China; [b]Department of gastroenterology and hepatology, Tianjin Medical University general hospital, Tianjin Medical University, Tianjin 300070, China; [c]Pasteurien College, Suzhou Medical College of Soochow University, Suzhou Key Laboratory of Pathogen Bioscience and Anti-infective Medicine, Suzhou, Jiangsu 215123, China; and [d]The School and Hospital of Stomatology, Tianjin Medical University, Tianjin 300070, China

Author contributions: Z.Y. and Q.W. designed research; K.Y., Q.L., X.S., X.P., Q.T., and X.D. performed research; H.C., L.Z., B.W., and W.Z. contributed new reagents/analytic tools; K.Y., Q.L., X.S., Z.Z., J.Y., J.L., R.L., C.M., Z.Y., and Q.W. analyzed data; and K.Y. and Q.W. wrote the paper.

Competing interest statement: K.Y., Z.Y., and Q.W. are co-inventors on patent application related to Ec-TMU and inflammatory bowel diseases.

This article is a PNAS Direct Submission. C.-j.G. is a guest editor invited by the Editorial Board.

[1]To whom correspondence may be addressed. Email: wangquan@tmu.edu.cn or yaozhi@tmu.edu.cn.

This article contains supporting information online at https://www.pnas.org/lookup/suppl/doi:10.1073/pnas.2309032120/-/DCSupplemental.

Published October 30, 2023.

In this study, we found *Ec*-TMU, a facultative anaerobic strain isolated from the feces of individuals treated by tinidazole (commonly used as a substitute for metronidazole), had a protective effect on DSS-induced colitis. We determined that indole-3-lactic acid (ILA) enriched in *Ec*-TMU supernatant alleviated intestinal inflammation via crosstalk between epithelia and macrophages. Mechanistically, we demonstrated that ILA inhibited glycolysis, NF-κB, and HIF pathways in epithelial cells to reduce CCL2/7 production, thereby preventing the accumulation of inflammatory macrophages.

Results

Gut Microbiota of Tinidazole Users Protects against DSS-Induced Colitis in Mice. To investigate the role of gut facultative anaerobes in intestinal homeostasis, we obtained feces from patients treated with tinidazole (a drug with anti-anaerobic activity similar to metronidazole that is commonly used for people after tooth extraction), and transplanted mice with fecal microbiota (FMT) for 7 d, followed by gavage with the fecal microbiota and 3.5% DSS in drinking water for another 7 d (Fig. 1*A*). We found that mice transplanted with the feces of tinidazole-treated patients were separated into two groups: those could ameliorate DSS-induced colitis (TNZ-L) and those had a similar effect (TNZ-S) compared with mice transplanted with the feces of healthy people, based on colon length, body weight, disease activity index (DAI) scores, and histopathological scores (Fig. 1 *B*–*E*).

To characterize the changes of gut microbial communities in people treated with tinidazole, we assessed the microbiota profiles of stool samples from people treated with tinidazole and healthy people in the above three groups via 16S rRNA gene analysis. The gut bacterial load and diversity of the control, TNZ-L, and TNZ-S groups did not differ significantly (*SI Appendix*, Fig. S1*A* and Fig. 1*F*). However, principle component analysis (PCA) revealed that the gut microbiota of the control, TNZ-L, and TNZ-S groups are separated into distinct clusters (Fig. 1*G*). Differences in the taxonomic composition of the three groups were observed at the genus level (Fig. 1*H*), and lots of different bacterial genera were present among the three groups (*SI Appendix*, Fig. S1*B*). The abundance of obligate anaerobes decreased and that of facultative anaerobes increased for the TNZ-L group compared with the other two groups (Fig. 1*I*). An annotated heatmap based on the abundant genera showed the clustering of the three groups, and fourteen genera were differentially enriched in the TNZ-L group, compared with either of the other two groups (Fig. 1 *J* and *K*). Of these genera, *Lactobacillus*, *Enterobacter*, *Enterococcus*, *Streptococcus*, and *Klebsiella* are facultative anaerobes (Fig. 1*K*). Interestingly, although most bacterial genera of the TNZ-L group are different from the fecal microbiota of mice treated with metronidazole (*SI Appendix*, Fig. S1*C*), four of the five elevated facultative anaerobic genera in the fecal microbiota of the TNZ-L group are the same as those of mice treated with metronidazole in our previous study (Fig. 1*L*). These results imply that these tinidazole-enriched facultative anaerobes have an effect on colitis remission.

***Ec*-TMU Alleviates DSS-Induced Colitis in Mice.** To obtain strains involved in colitis remission, seven isolated strains belonging to the five elevated genera from the feces of the TNZ-L group were used to investigate their anti-inflammatory effects in a DSS-induced colitis mouse model (Fig. 2*A*). An *Escherichia coli* strain (named *Ec*-TMU) and a *Klebsiella singaporensis* strain were found to reduce colitis in mice, with *Ec*-TMU having a greater anti-inflammatory impact than *K. singaporensis* (Fig. 2 *B*–*E* and *SI Appendix*, Fig. S1 *D*–*G*). *E. coli* K12 was also used as a control since it belongs to the same bacterial species as *Ec*-TMU. The effect of *Ec*-TMU existed in the model even without strain pretreatment (Fig. 2 *F*–*J*). Moreover, we validated the anti-inflammatory effect of *Ec*-TMU in germ-free (GF) mice (Fig. 2 *K*–*O*). This observation suggests that *Ec*-TMU exerts its anti-inflammatory properties in mice with DSS-induced colitis without the presence of other bacteria.

We further evaluate the effect of *Ec*-TMU on DSS-induced colitis in the presence of gut microbiota. In the mouse model with or without strain pretreatment, mice in the *Ec*-TMU group showed lower DAI scores, longer colons, and lower histological scores (*SI Appendix*, Fig. S2 *A*–*J*). To determine whether *Ec*-TMU gavage is harmful to mice, we measured body weight, DAI, colon length, and pathological changes in the colon, kidney, liver, and lung (*SI Appendix*, Fig. S2 *K*–*R*).

Then, we investigated the effect of *Ec*-TMU on the intestinal epithelial barrier in the mouse model with a single bacterial colonization (Fig. 2*A*). In accordance with reduced colitis, *Ec*-TMU induced increased expression of Muc2 (mucus protein) and Occluding (tight junction protein), increased goblet cells and Ki67$^+$ cells, but decreased cleaved caspase 3$^+$ apoptotic cells, while no difference was observed for the expression of Lgr5 (stem cell marker) (*SI Appendix*, Fig. S3 *A*–*F*). Lower plasma levels of FITC-conjugated dextran confirmed reduced intestinal barrier permeability after *Ec*-TMU treatment (*SI Appendix*, Fig. S3*M*). However, *Ec*-TMU gavage had no effect on Muc2, Occluding, goblet/Ki67$^+$/Lgr5/cleaved caspase 3$^+$ cell (*SI Appendix*, Fig. S3 *G*–*L*), without DSS treatment (*SI Appendix*, Fig. S2*K*), indicating that *Ec*-TMU does not influence the intestinal epithelial barrier in homeostasis.

Taken together, these results demonstrate that *Ec*-TMU reduces the susceptibility of mice to DSS-induced colitis in several models and has no direct effect on the intestinal barrier.

***Ec*-TMU Suppresses the Accumulation of Pro-Inflammatory Macrophages during DSS-Induced Colitis.** Due to the importance of immune cells in IBD pathogenesis, we explored the immune cells in the intestinal microenvironment affected by *Ec*-TMU during DSS-induced colitis. In the above mouse model with a single bacterial colonization (Fig. 2*A*), *Ec*-TMU had no obvious effect on the percentage and number of DCs, CD103$^+$DCs, Teffs, and Tregs in mesenteric lymph nodes (MLN) (*SI Appendix*, Fig. S4 *A*–*G*) and ILC3s in colonic lamina propria (cLP) (*SI Appendix*, Fig. S5 *A* and *B*). However, the number and percentage of macrophages showed a declining trend in the *Ec*-TMU group compared with that in the other two groups (*SI Appendix*, Fig. S5*C*). The number and percentage of neutrophils were reduced in the *Ec*-TMU group compared with that in the control group (*SI Appendix*, Fig. S5 *D* and *E*). We further analyzed the four subsets of macrophages including pro-inflammatory P1/P2 and anti-inflammatory P3-P4 in the mice treated with *Ec*-TMU or *K12* (*SI Appendix*, Fig. S5*D*). The percentage and number of macrophages in cLP were reduced in the *Ec*-TMU group compared with the control and *K12* groups (Fig. 3*A*). The percentage and number of pro-inflammatory macrophages (P1/P2) were significantly decreased, whereas the percentage of anti-inflammatory P3-P4 macrophages had an increased trend in the *Ec*-TMU group (Fig. 3*C*). Consistent with the increased percentage of anti-inflammatory P3-P4 macrophages, the percentage of CX3CR1$^+$ macrophages showed an increased trend in the *Ec*-TMU group (Fig. 3*B*). Taken together, these results indicate that *Ec*-TMU reduces the accumulation of pro-inflammatory macrophages in the colitis-related intestinal microenvironment.

***Ec*-TMU Metabolites Regulate CCL2 and CCL7 Expression in Colonic Epithelial Cells.** Chemokines produced by intestinal epithelial cells or macrophages during inflammation play crucial

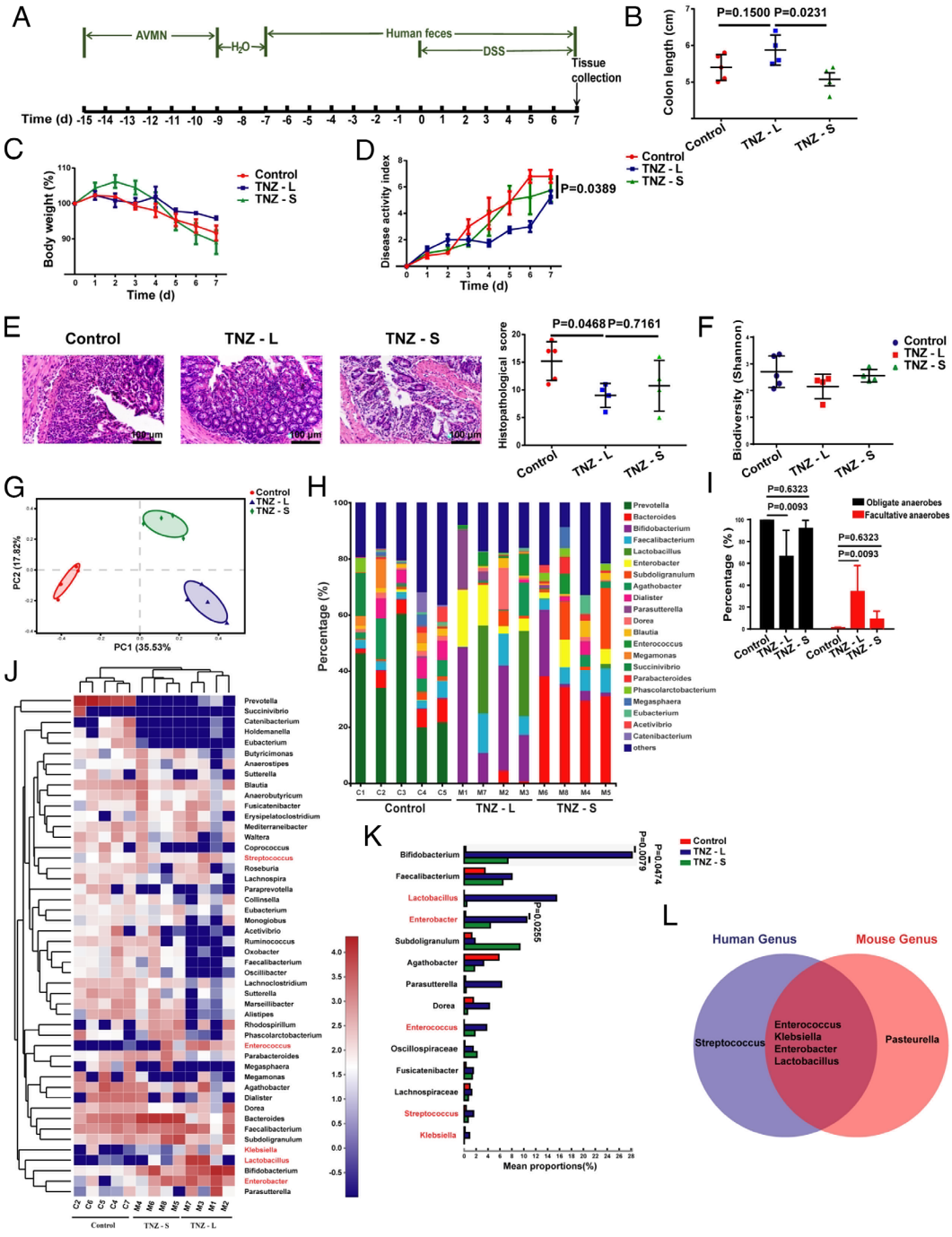

Fig. 1. The stool of some people treated with tinidazole protects mice against DSS-induced colitis. (*A*) Schematic diagram for the mouse model of DSS-induced acute colitis combined with FMT. Mice were gavaged daily with stool from people treated with tinidazole or healthy people for 14 d after 6 d of a combination of ampicillin, vancomycin, neomycin, and metronidazole (AVMN) and 2 d of water treatment. After 7 d of stool gavage, mice were given 3.5% DSS simultaneously to induce colitis for 7 d, and mice were killed. (*B–E*) Analysis of colon length (*B*), body weight (*C*), disease activity index (*D*), and histopathological score (*E*) post DSS administration for the control, TNZ-L group, and TNZ-S group. Bacterial DNA collected from stool of people treated with tinidazole and healthy people was used to perform 16S rRNA gene sequencing. (*F*) Alpha diversity (Shannon index) of bacteria for the control, TNZ-L group, and TNZ-S group. (*G*) Beta diversity of bacteria for the control, TNZ-L group, and TNZ-S group. (*H*) The mean relative abundance at the genus level of bacteria for the control, TNZ-L group, and TNZ-S group. (*I*) Percentages of the obligate anaerobic bacteria and facultative anaerobic bacteria in the control, TNZ-L group, and TNZ-S group. (*J*) Heatmap depiction of the mean relative abundance of bacteria at the genus level for the control, TNZ-L group, and TNZ-S group. The genus marked in red are facultative anaerobic bacteria. (*K*) Genus with higher content in the TNZ-L group A than either of the other two groups. (*L*) Venn diagram indicating facultative anaerobic bacteria genus enriched in the stool samples from people treated with tinidazole and mice treated with metronidazole. n = 5 or 4 in each group. Data are the mean ± SEM, two-way ANOVA (*C* and *D*), or one-way ANOVA (*B*, *E*, *F*, *I*, and *K*).

roles in pro-inflammatory macrophage accumulation. We then investigated the effect of *Ec*-TMU on related chemokine expression in macrophages and epithelial cells in vitro. Live *Ec*-TMU has no specific effect on the mRNA levels of several chemokines except for *Ccl5* in bone marrow–derived macrophages (BMDMs) stimulated by LPS (*SI Appendix*, Fig. S6 *A–F*). Meanwhile, live *Ec*-TMU (MOI = 5) obviously reduced the mRNA levels of *Ccl2* and *Ccl7* in colonic epithelial cells stimulated by LPS (*SI Appendix*, Fig. S6 *G–M*). The mRNA levels of *Ccl2/7* in colon tissues of mice treated by *Ec*-TMU during DSS-induced colitis were found to be decreased compared with those in the other groups (Fig. 4*A*). In addition, the CCL2/7 protein levels in colon tissues were significantly decreased in the *Ec*-TMU group compared with the other two groups (Fig. 4 *B* and *C*). Accordingly, we found pro-inflammatory macrophages expressing CCR2 (the chemokine receptor for CCL2/7), but not CCR5 (the chemokine receptor for CCL5), were decreased in the *Ec*-TMU group (Fig. 4 *D* and *E*). Collectively, these results suggest that *Ec*-TMU decreases the production of CCL2/7 in epithelial cells.

We next assessed the effect of the heat-killed bacteria and bacterial products on the epithelial cells. *Ec*-TMU supernatant decreased *Ccl2* and *Ccl7* mRNA levels in SW480 cells (Fig. 4 *F* and *G*); however, heat-killed *Ec*-TMU had no effect on CCL2/7 (*SI Appendix*, Fig. S6 *N* and *O*). The supernatant was further separated into six kinds of molecular weight fractions (≥100/50/30/10/3 and <3 kDa), and the <3 kDa fraction, but not other fractions of the *Ec*-TMU supernatant, significantly suppressed *Ccl2* and *Ccl7* mRNA levels (Fig. 4*H* and *SI Appendix*, Fig. S6 *P* and *Q*). In addition, the CCL2/7 protein level in SW480 cells stimulated by LPS was significantly reduced by *Ec*-TMU supernatant (<3 kDa) treatment (Fig. 4 *I* and *J*). Together, these data demonstrate that *Ec*-TMU supernatant (<3 kDa) reduces CCL2 and CCL7 expression in colonic epithelial cells stimulated by LPS.

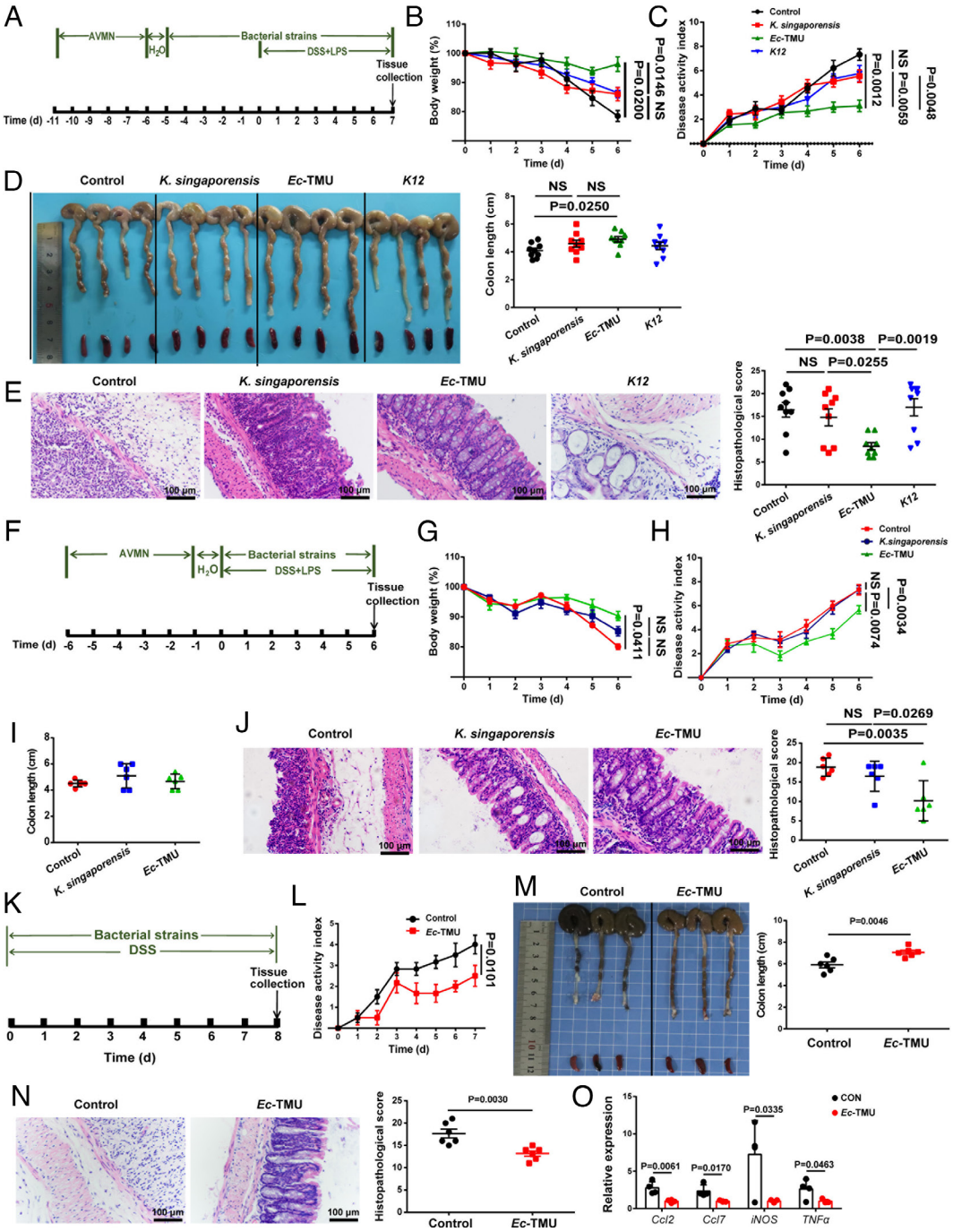

Fig. 2. *Ec*-TMU protects mice against DSS-induced colitis. (*A*) Schematic diagram for the mouse model to detect the prophylactic effect of single bacteria on colitis. Mice were gavaged daily with 10^9 CFU of *K. singaporensis*, *Ec*-TMU, *K12*, or sterile water after 5 d of AVMN and one day of water treatment. After 5 d of single bacterial strain pretreatment, mice were given 3.5% DSS and LPS (8 mg/kg body weight) simultaneously to induce colitis in addition with single bacteria administration for another 7 d. (*B–E*) Analysis of body weight (*B*), disease activity index (*C*), colon length (*D*), and histopathological scores (*E*) in each group. (*F*) Schematic diagram for the mouse model to detect the therapeutic effect of single bacteria on colitis. Mice were gavaged daily with 10^9CFU of *K. singaporensis*, *Ec*-TMU or sterile water after 5 d of AVMN and 1 d of water treatment. Then, mice were given 3.5% DSS and LPS (8 mg/kg body weight) simultaneously to induce colitis in addition with single bacterial strain administration for another 7 d. (*G–J*) Analysis of body weight (*G*), disease activity index (*H*), colon length (*I*), and histopathological scores (*J*) in each group. (*K*) Schematic diagram for the mouse model to detect the therapeutic effect of single bacteria on DSS-induced colitis in germ-free mice. Mice were daily gavaged with 10^9 CFU of each strain or water in addition with 2.5% DSS exposing for 8 d, and mice were killed. (*L–N*) Analysis of disease activity index (*L*), colon length (*M*), and histopathological scores (*N*) in each group. (*O*) mRNA expression levels of inflammatory cytokines in the colon of germ-free mice. (*B–E*) n = 9 in each group. (*G–J* and *L–N*) n = 6 in each group. (*O*) n = 4 in each group. Data are the mean ± SEM, two-way ANOVA (*B*, *C*, *G*, *H*, and *L*), one-way ANOVA (*D*, *E*, *I*, and *J*), or unpaired Student's *t* test (*M–O*). NS, not significant.

***Ec*-TMU-Derived Indole-3-lactic Acid Has a Therapeutic Effect on DSS-Induced Colitis.** The <3-kDa fraction of *Ec*-TMU supernatant was analyzed using LC-MS to determine its potential anti-inflammatory metabolites. PCA showed that metabolites from the BHI (Brain Heart Infusion medium), *Ec*-TMU, and K12 groups are separated into distinct clusters (*SI Appendix*, Fig. S6*R*). Compared with the BHI and K12 groups, 77 metabolites were significantly upregulated (fold change > 1, $P < 0.05$) and 82 were significantly downregulated (fold change < 1, $P < 0.05$) in the *Ec*-TMU group, and several tryptophan and tyrosine derivatives were increased in the *Ec*-TMU group (Fig. 5 *A* and *B*). KEGG pathway analysis showed metabolites were mainly enriched in tryptophan metabolism and tyrosine metabolism pathways (Fig. 5 *C* and *D*). We then focused on the four derivatives of tryptophan and tyrosine significantly upregulated in the *Ec*-TMU group: 5-methoxytryptophan (5-MTP), hydroxyphenyllactic acid (HPLA), kynurenic acid (KynA), and indole-3-lactic acid (ILA).

Compared with the other three metabolites, ILA inhibited both the *Ccl2* and *Ccl7* mRNA levels in LPS-stimulated SW480 cells more effectively (Fig. 5*E* and *SI Appendix*, Fig. S6 *S–U*). The concentration of ILA in the *Ec*-TMU supernatant (<3 kDa) was significantly higher than that in the *K. singaporensis* or K12 supernatant (Fig. 5*F*). After fecal microbiota transplantation with healthy human feces, TNZ treatment increased ILA levels in mouse feces (*SI Appendix*, Fig. S7*A*). In addition, *Ec*-TMU gavage increased ILA concentration in mouse feces (*SI Appendix*, Fig. S7*B*). CCL2 and CCL7 protein levels in LPS-stimulated SW480 cells were also downregulated by ILA (Fig. 5 *G* and *H*).

We subsequently found that ILA has a therapeutic effect on alleviating DSS-induced colitis in mice (Fig. 5 *I–M*). In addition,

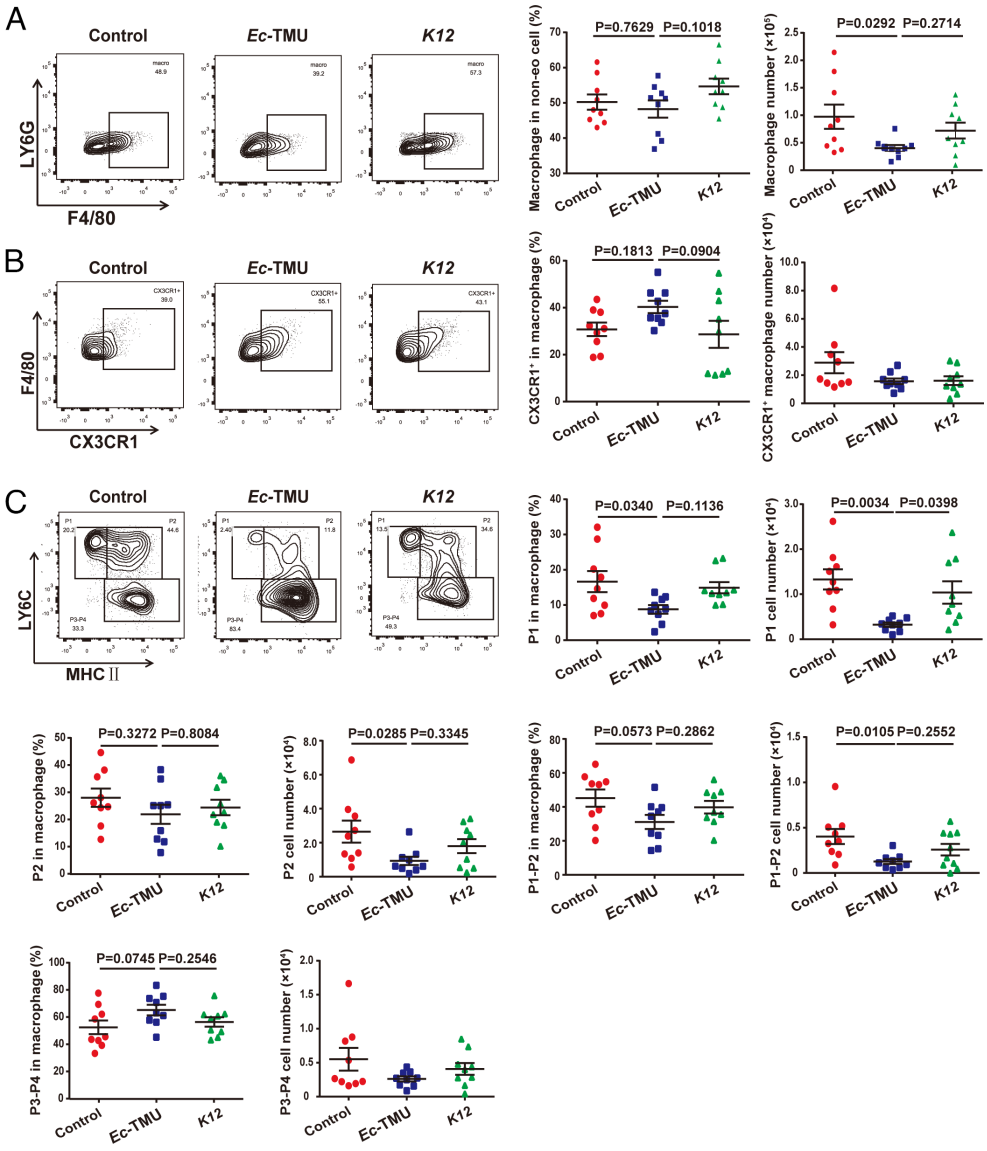

Fig. 3. *Ec*-TMU decreases inflammatory macrophages in cLP. cLP of mice (in the model of Fig. 2*A*) from the *Ec*-TMU, *K12* or control groups were collected, and lymphocytes were analyzed using flow cytometry. (*A*) The percentage of macrophages in non-eosinophilic (non-eo) cells and the number of macrophages in cLP. (*B*) The percentage of $CX3CR1^+$ macrophages in macrophages and the number of $CX3CR1^+$ macrophages in cLP. (*C*) The percentage of P1-P4 subsets in total macrophages and the number of P1 to P4 in cLP. n = 9 (*A–C*). Data are the mean ± SEM, one-way ANOVA.

decreased mRNA levels of inflammatory factors (*Il-6*, *Cxcl1*, *iNOS*, *Tnf-α*, *Il-1β*, *Ccl2,* and *Ccl7*), increased goblet cells, and an Occluding protein level were observed in the colons treated by ILA (Fig. 5*N* and *SI Appendix*, Fig. S7 *C* and *D*). However, ILA did not show a prophylactic effect on protecting against DSS-induced colitis (*SI Appendix*, Fig. S7 *E–I*).

Additionally, we examined immune cells in the intestinal microenvironment during colitis treated by ILA. Macrophages, neutrophil, and Th17 cells were significantly reduced in the cLP of the ILA group (*SI Appendix*, Fig. S7 *J–P* and *W*). No significant difference was observed in the percentage and number of DCs, $CD103^+$DCs, Tregs, and Th1 cells (*SI Appendix*, Fig. S7 *Q–T*), and decreased Th2 and Th17 cells were observed in the MLN (*SI Appendix*, Fig. S7 *U* and *V*). Moreover, the percentages of pro-inflammatory macrophages (P1/P2) decreased and anti-inflammatory P3-P4 or $CX3CR1^+$ macrophages increased in the ILA group (Fig. 5*O* and *SI Appendix*, Fig. S7 *X* and *Y*). We also observed that $CCR2^+$ P1/P2 macrophages decreased in the ILA group (Fig. 5*P*). The CCL2/7 protein levels in the colons of ILA-treated mice during colitis were obviously reduced (Fig. 5 *Q* and *R*).

To investigate the role of pro-inflammatory macrophages in the effect of ILA on DSS-induced colitis, we used clodronate liposomes (CLP) to induce macrophage depletion in mice (*SI Appendix*, Fig. S8*A*). After CLP treatment, the inflammation was decreased, and ILA showed no effect on the DSS-induced colitis remission (*SI Appendix*, Fig. S8 *B–E*). In addition, ILA had no effect on decreasing macrophages, Th2, or Th17 cells in CLP-treated mice (*SI Appendix*, Fig. S8 *F–J*). Meanwhile, the effect of ILA on colitis was not eliminated by neutrophil depletion (*SI Appendix*, Fig. S8 *K–P*). Moreover, we examined the role of $CCR2^{+/+}$ macrophages and found that ILA's effect on DSS-induced colitis was eliminated in $CCR2^{-/-}$ mice, but the effect of ILA was restored after the adoptive transfer of $CCR2^{+/+}$ macrophages from wild-type mice into $CCR2^{-/-}$ mice (*SI Appendix*, Fig. S9 *A–D*).

We further evaluate whether ILA affects gut microbiota using 16S rRNA sequencing (PRJNA945177) (15). Principle component analysis showed that microbiota of the control and ILA groups were not clustered separately (*SI Appendix*, Fig. S9*E*), and no significant differences were found based on the Shannon diversity index (*SI Appendix*, Fig. S9*F*). The abundance of the dominant bacteria in the two groups is similar at the phylum, order, family, and genus levels (*SI Appendix*, Fig. S9 *G* and *H*).

These results suggest that ILA decrease pro-inflammatory macrophage accumulation during colitis through inhibiting CCL2/7 expression in epithelial cells, thereby alleviating DSS-induced colitis.

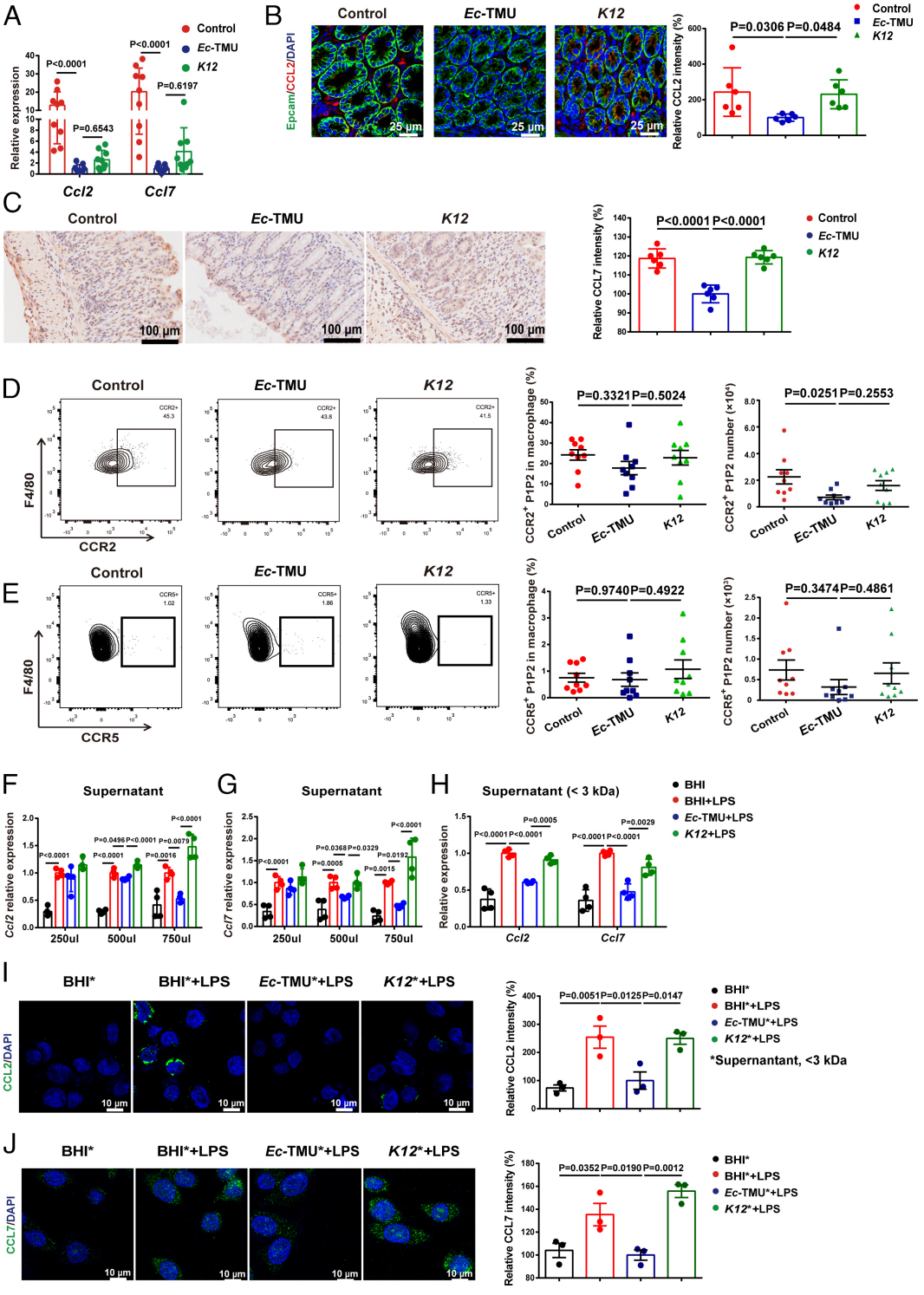

Fig. 4. *Ec*-TMU supernatant reduces CCL2/7 expression in epithelial cells. On day 7, mice were killed in the model of Fig. 2*A*. (*A*) mRNA expression levels of *Ccl2* and *Ccl7* in the colons. (*B*) Immunofluorescence analysis of CCL2 expression in mouse colons. (Scale bar: 25 μm.) Blue, nucleus; green, Epcam; red, CCL2. (*C*) Immunohistochemical analysis of CCL7 expression in mouse colons. (Scale bar: 100 μm.) Lymphocytes in cLP of mice from the *Ec*-TMU, K12, or control groups were analyzed. (*D*) The percentage and number of $CCR2^+$ macrophages in cLP. (*E*) The percentage and number of $CCR5^+$ macrophages in cLP. (*F* and *G*) SW480 cells were stimulated with bacteria culture supernatant and LPS (10 μg/mL) for 3 h. mRNA levels of *Ccl2* (*F*) and *Ccl7* (*G*) were evaluated for cells incubated with BHI broth, *Ec*-TMU, and *K12* culture supernatant. (*H–J*) SW480 cells were simultaneously stimulated with bacteria culture supernatant (750 μL, <3 kDa) and LPS (10 μg/mL) for 3 h. (*H*) mRNA levels of *Ccl2* and *Ccl7* were evaluated for cells incubated with BHI, BHI+LPS, *Ec*-TMU culture supernatant (<3 kDa) + LPS, or *K12* culture supernatant (<3 kDa) + LPS. (*I* and *J*) Immunofluorescence analysis of CCL2 (*I*) and CCL7 (*J*) in cells. Asterisks indicate <3-kDa fractions of bacterial supernatant. CCL2 and CCL7: green; DAPI: blue. (Scale bar: 10 μm.) n = 9 (*A*, *D*, and *E*), n = 6 (*B* and *C*), n = 4 (*F–H*) and n = 3 (*I* and *J*) in each group. Data are the mean ± SEM, one-way ANOVA.

ILA Inhibits CCL2 and CCL7 Expression during Inflammation by Regulating HIF, NF-κB Signaling Pathway, and Glycolysis. To investigate the underlying molecular mechanism of the ILA effect on CCL2/7 expression, we examined the gene expression profiles of SW480 cells treated by LPS and *Ec*-TMU supernatant (<3 kDa) using RNA sequencing (PRJNA946043) (16). There were 612 genes upregulated and 281 genes downregulated in the SW480 cells treated with LPS and BHI (<3 kDa) compared with that treated with BHI (<3 kDa) ($P < 0.05$ and fold change > 1), including *Ccl2* and *Ccl7* (*SI Appendix*, Fig. S10*A*). KEGG analysis showed that several inflammatory signaling pathways were upregulated (*SI Appendix*, Fig. S10*B*). Furthermore, there were 2100 genes upregulated and 2158 genes downregulated in the SW480 cells treated with LPS and *Ec*-TMU supernatant (<3 kDa) compared with that treated with LPS and BHI (<3 kDa) ($P < 0.05$ and fold change > 1) (*SI Appendix*, Fig. S10*C*), and the HIF and NF-κB signaling pathways are the top two downregulated pathways (*SI Appendix*, Fig. S10*D*). In addition, the expression of genes associated with glycolysis, HIF, and NF-κB signaling pathways, such as *Ldha*, *Hk2*, *RelA*, *Ifngr2*, *Nfkb1*, and *Nfkb2*, was downregulated in the *Ec*-TMU group (*SI Appendix*, Fig. S10 *E–G*).

We further performed RNA-seq analysis of SW480 cells treated by LPS and ILA (PRJNA946045) (17). LPS stimulation induced chemokine gene expression in SW480, such as *Ccl2, Ccl5, Ccl7,*

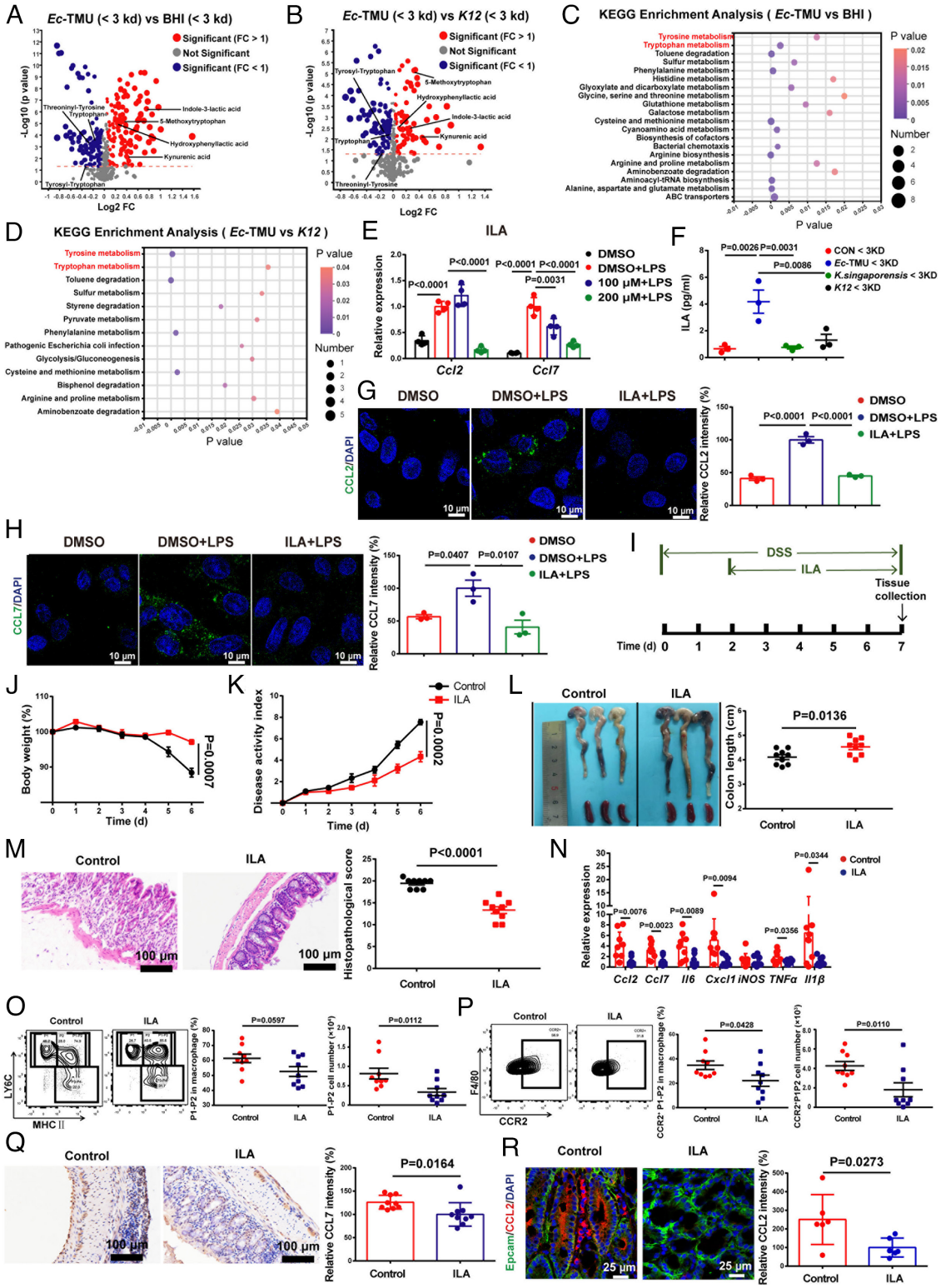

Fig. 5. ILA from *Ec*-TMU protects mice against DSS-induced colitis. (*A* and *B*) The fold change and p-value distribution of metabolites (<3 kDa) from *Ec*-TMU culture supernatant, compared with BHI (*A*) or *K12* culture supernatant (*B*). (*C* and *D*) KEGG analysis of the upregulated metabolic pathways based on metabolites (<3 kDa) from *Ec*-TMU culture supernatant, compared with BHI (*C*) or K12 (*D*) culture supernatant. (*E*) SW480 cells were stimulated with PBS, LPS (6 μg/mL) in addition with DMSO, 100 μM, or 200 μM ILA (6 h), and mRNA levels of Ccl2 and Ccl7 were evaluated. (*F*) Analysis of ILA levels in the BHI, *Ec*-TMU, *Klebsiella singaporensis* and K12 culture supernatant (<3 kDa). (*G* and *H*) Immunofluorescence analysis of CCL2 (*G*) and CCL7 (*H*) in cells incubated with LPS (6 μg/mL) in addition with ILA (200 μM) or DMSO for 6 h. CCL2 or CCL7: green; DAPI: blue. (Scale bar: 10 μm.) (*I*) Schematic diagram for the mouse model of DSS-induced acute colitis combined with ILA treatment. After 2 d of 3.5% DSS administration, mice were daily gavaged with sterile water or 40 mg/kg ILA. (*J*–*M*) Analysis of body weight (*J*), disease activity index (*K*), colon length (*L*), and histopathological scores (*M*) in each group. (*N*) mRNA expression levels of inflammatory cytokines in the colon. (*O*–*R*) At day 7 (in the model of Fig. 5*I*), cLP of mice were collected, and lymphocytes were analyzed using flow cytometry. Colon tissues were stained and analyzed. (*O*) The percentage and the number of inflammatory (P1/P2) subsets in cLP. (*P*) The percentage and the number of $CCR2^{+}$ P1/P2 macrophages in cLP. (*Q*) Immunohistochemical analysis of CCL7 expression in mouse colons. (Scale bar: 100 μm.) (*R*) Immunofluorescence analysis of CCL2 in mouse colons. (Scale bar: 25 mm.) Blue, nucleus; green, Epcam; red, CCL2. n = 3 (*A*–*D* and *F*–*H*), n = 4 (*E*), n = 9 (*J*–*Q*), n = 6 (*R*) in each group. Data are the mean ± SEM. One-way ANOVA (*E*–*H*), two-way ANOVA (*J* and *K*), and unpaired Student's *t* test (*L*–*R*).

and *Ccl20* (*SI Appendix*, Fig. S10*H*), and the upregulated genes were enriched in signaling pathways including HIF and NF-κB (*SI Appendix*, Fig. S10*I*). There were 427 genes upregulated (such as AHR target genes) and 440 genes downregulated (such as chemokine genes) in the SW480 cells treated with LPS and ILA compared with those treated with LPS ($P < 0.05$ and fold change > 1) (Fig. 6*A*). Downregulated genes were mainly enriched in signaling pathways, including HIF and NF-κB, and also glycolysis for the ILA group (Fig. 6 *B*–*E*).

In the mouse model (Fig. 5*I*), we also observed that ILA gavage decreased glycolysis, and the protein levels of HIF1α and p-IκBα (Fig. 6 *F*–*H*), while simultaneously increasing the AHR target protein CYP1A1 in the colon (*SI Appendix*, Fig. S10*J*). In vitro experiments, ILA showed no effect on decreasing *Ccl2* and *Ccl7* mRNA levels in LPS-stimulated SW480 cells in the presence of the NF-κB inhibitor (BAY 11-7085), NF-κB agonist (PMA), glycolysis inhibitor (DCA), glycolysis agonist (oligomycin), HIF inhibitor (PX-478), HIF agonist (ML228), or AHR inhibitor (CH-223191) (Fig. 6 *I*–*O*). Moreover, ILA-decreased HIF1α and p-IκBα production, and glycolysis was found to be AHR-dependent (Fig. 6 *P* and *Q*). In addition, the NF-κB inhibitor and HIF inhibitor treatment abrogated the effect of ILA on glycolysis by evaluating the mRNA expression of key enzymes involved in glycolysis or extracellular acidification rate (ECAR) analysis (Fig. 6 *R* and *S*).

These results indicate that ILA decreases CCL2 and CCL7 expression through AHR, NF-κB/HIF signaling pathways, and glycolysis, and interestingly, the interaction between HIF/NF-κB signaling pathways and glycolysis was observed.

The CCL2/7- CCR2 Axis and ILA Content Are Associated with IBD Progression. To validate the role of ILA, CCL2/7, and CCR2 in the development of IBD, we examined the fecal ILA levels in 12 ulcerative colitis (UC) patients (PRJNA946039) (18), and a negative correlation was observed between fecal ILA and calprotectin (the marker of inflammation for predicting the clinical relapse of ulcerative colitis), but the correlation between fecal ILA and blood CRP (the system inflammation indicator) was not strong (Fig. 7 *A* and *B*). The aromatic lactate dehydrogenase (ALDH) from *Bifidobacterium* species is identified to be involved in ILA synthesis (19); therefore, we analyzed the abundance of the gene encoding ALDH in fecal microbiota using available metagenomic data from NCBI: HMP (PRJNA43017, PRJNA275349, PRJNA306874), Cardiff cohort (PRJEB7949), and PRISM/STINKI cohorts (PRJNA385949). A trend of decreased *aldh* gene abundance was observed in IBD patients compared with healthy people, and the significance was found for one cohort (Fig. 7*C*). Moreover, we analyzed CCL2/7 expression in epithelia and CCR2 expression in macrophages using available single-cell RNA sequencing data from colon biopsies of UC patients (Single Cell Portal accession SCP259). CCL2/7 expression in epithelia and CCR2 expression in macrophages are significantly higher in UC patients than in healthy individuals. (Fig. 7 *D*–*E*). These clinical investigations correspond to the role of ILA in reducing inflammation and the involvement of epithelial CCL2/7 and macrophage CCR2 during colitis.

Discussion

This study demonstrates that ILA reduces susceptibility to DSS-induced colitis and regulates intestinal homeostasis in mice by inhibiting the crosstalk between intestinal epithelia and macrophages (Fig. 7*F*). This sheds light on the interaction between bacteria-derived compounds and the immune system in the inflamed intestine.

During intestinal inflammation, blood-derived $LY6C^{hi}$ monocytes are more inclined to differentiate into $LY6C^{int}CX3CR1^{int}$ cells that secrete more inflammatory cytokines including IL-12, IL-23, and IL-1β, consequently leading to effector T cell immune responses and exacerbating inflammatory damage (20). Targeting macrophages may improve IBD treatment (21). Corticosteroids and 5-aminosalicylates, for instance, suppress intestinal inflammatory macrophages directly (22). Anti-TNF, one of the most important treatments, induces alternative macrophage polarization, which repairs tissue damage (23). ILA demonstrated a therapeutic but not a preventative effect on DSS-induced colitis, which is different from *Ec*-TMU. It is possible that the wide spectrum of anti-inflammatory actions of *Ec*-TMU are related to the synthesis of various metabolites, one of which is ILA. We demonstrate that ILA-reduced macrophage accumulation further influenced Th2 and Th17 infiltration in the mice intestine, thereby altering intestinal cell interactions to promote gut homeostasis and protect against colitis.

The interaction between chemokines and receptors regulates blood-derived monocyte migration to the inflammatory colon. Upregulated Fbxw7 in colon macrophages stimulates CCL2 and CCL7 production to recruit more inflammatory mononuclear phagocytes, worsening colitis (24). In an epithelial-derived CCL2-dependent mechanism, gut microbiota LPS recruits monocyte-like macrophages to develop colitis-associated tumors (25). To minimize intestinal inflammation and macrophage buildup, CCL2/7 production must be controlled. NF-κB, HIF, and glycolysis regulate CCL2/7 synthesis (26–30). AHR promotes stem cell differentiation and tight junction protein production in IECs (31), but its effect on chemokine production is less studied. In this study, ILA-activated AHR in IECs inhibits the NF-κB and HIF signaling pathways and glycolysis, reducing CCL2/7 production and pro-inflammatory macrophage accumulation.

ILA, a bacterial tryptophan derivative, activates AHR and Nrf-2 to reduce LPS-induced mature IEC inflammation (32). ILA exhibits anti-inflammatory activity by upregulating AHR and STAT1 pathways in IL-1β or LPS-inflamed immature epithelial cells (33, 34). Recently, *L. reuteri*–produced ILA has been shown to have a significant effect on inhibiting colorectal cancer by reducing Th17 cells through targeting the nuclear receptor, RAR-related orphan receptor γt (RORγt) (35). *L. plantarum*–derived ILA upregulates IL12a production in dendritic cells by increasing H3K27ac binding at IL12a enhancer regions and transcriptionally inhibit Saa3 expression related to $CD8^+$ T cell cholesterol metabolism, which improves tumor-infiltrating $CD8^+$ T cell function and alleviates colorectal cancer (36). However, the role and mechanism of ILA in colitis are uncertain. We found that ILA inhibits glycolysis, HIF, and NF-κB pathways in epithelia and further inhibits CCL2/7 production, which involves signaling pathway-metabolism interaction. Animal and clinical findings demonstrate that ILA can treat advanced colitis and predict IBD development. To test ILA for IBD diagnosis and treatment, the clinical sample size should be increased in future research.

Collectively, our findings show a potential relationship between the metabolites of gut microbiota, epithelium, and pathogenic immune responses in the colon and provide unique insights for the future diagnosis and treatment of IBD.

Materials and Methods

Mice. Wild-type male C57BL/6J mice were purchased from the Academy of Military Medical Science (Beijing, China). Germ-free C57BL/6J mice were obtained from GemPharmatech (Nanjing, China) and maintained in flexible-film isolators in the GemPharmatech. CCR2-KO mice (Strain NO.T029128) were purchased from GemPharmatech (Nanjing, China) (*SI Appendix*, Table S1). All mice except GF mice were maintained under specific pathogen-free conditions

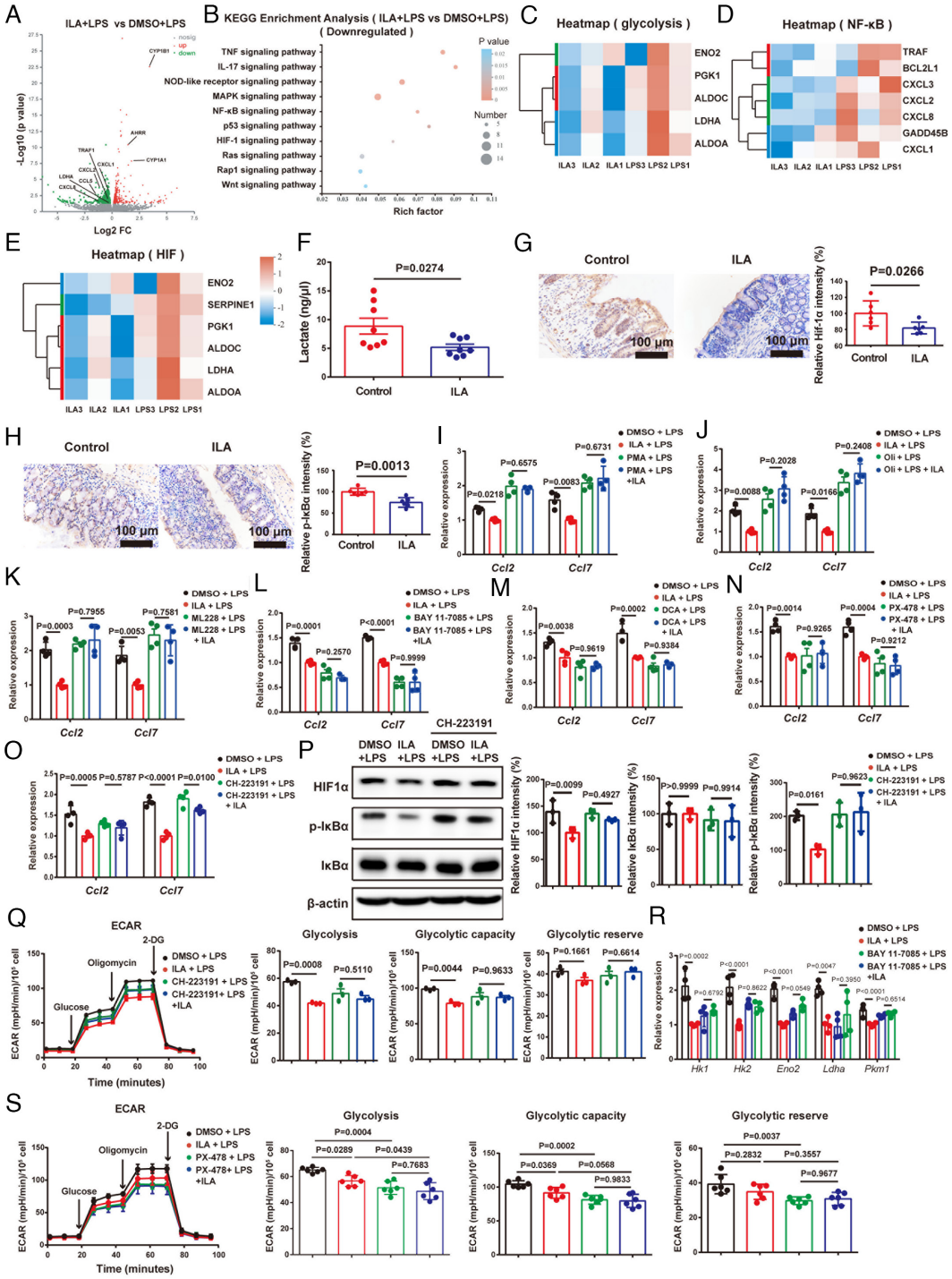

Fig. 6. ILA decreases CCL2 and CCL7 expression in epithelial cells through downregulating HIF, NF-κB pathways and glycolysis. (*A–E*) RNA-seq analysis of SW480 cells treated with PBS or LPS (6 μg/mL) in addition with DMSO or ILA (200 μM) for 6 h. (*A*) Volcano plot showing the upregulated and downregulated genes in SW480 cells. (*B*) KEGG analysis of cells. (*C–E*) Heatmap depiction of gene expression involved in glycolysis (*C*), NF-κB (*D*), HIF (*E*) signaling pathways. (*F–H*) At day 7 (in the model of Fig. 5*I*), colon tissues were collected, stained, and analyzed. (*F*) The lactate content of isolated colonocytes. (*G* and *H*) Immunohistochemical analysis of HIF1α (*G*) and p-IκBα (*H*) expression in colonic tissues. (Scale bar: 100 μm.) (*I–K*) SW480 cells were pretreated with DMSO, NF-κB agonist [Phorbol 12-myristate 13-acetate (PMA), 100 nM] (*I*) for 4 h, subsequently stimulating cells with DMSO or ILA (400 μM) for another 12 h. After 16 h, cells are stimulated with 6 μg/mL LPS for 6 h. SW480 cells were pretreated with DMSO, glycolysis agonist (oligomycin, 5 nM) (*J*), HIF agonist (ML-228, 10 nM) (*K*) for 3 h, subsequently stimulating cells with DMSO or ILA (400 μM) for another 6 h. After 9 h, cells are stimulated with 2 μg/mL LPS for 3 h. mRNA levels of *Ccl2* and *Ccl7* were evaluated. (*L–O*) SW480 cells were pretreated with DMSO, NF-κB inhibitor (BAY 11-7085, 1 μM) (*L*), glycolysis inhibitor (DCA, 10 mM) (*M*), HIF inhibitor (PX-478, 1 μM) (*N*), or AHR inhibitor (CH-223191, 10 μM) (*O*) for 4 h, subsequently stimulating cells with DMSO or ILA (400 μM) for another 12 h. After 16 h, cells are stimulated with 6 μg/mL LPS for 6 h. mRNA levels of *Ccl2* and *Ccl7* were evaluated. (*P*) The treatment process was the same as Fig. 6*O*. The HIF1α, p-IκBα and IκBα density in SW480 cells was normalized to that of β-Actin. The relative density of the DMSO group was set to 100%. (*Q*) The treatment process was the same as Fig. 6*O*. ECAR analysis of ILA and CH-223191 effect on glycolysis of SW480 cells. ECAR levels were measured following sequential treatments with glucose (10 mM), oligomycin (2 μM), and 2-DG (50 mM) for calculating glycolysis, glycolysis capacity, and glycolytic reserve. (*R*) SW480 cells were pretreated with DMSO or NF-κB inhibitor (BAY 11-7085, 5 μM) for 4 h, subsequently stimulating cells with DMSO or ILA (400 μM) for another 12 h. After 16 h, cells are stimulated with 6 μg/mL LPS for 6 h. mRNA levels of *Hk1, Hk2, Eno2, Ldha,* and *Pkm1* were evaluated. (*S*) ECAR analysis of ILA and PX-478 effect on glycolysis of SW480 cells. ECAR levels were measured following sequential treatments with glucose (10 mM), oligomycin (2 μM), and 2-DG (50 mM) for calculating glycolysis, glycolysis capacity, and glycolytic reserve. n = 3 (*A–E*, *P*, and *Q*), n = 8 (*F*), n = 6 (*G*, *H*, and *S*), n = 4 (*I–O* and *R*) in each group. Data are the mean ± SEM. Unpaired Student's *t* test (*F–H*) and one-way ANOVA (*I–S*).

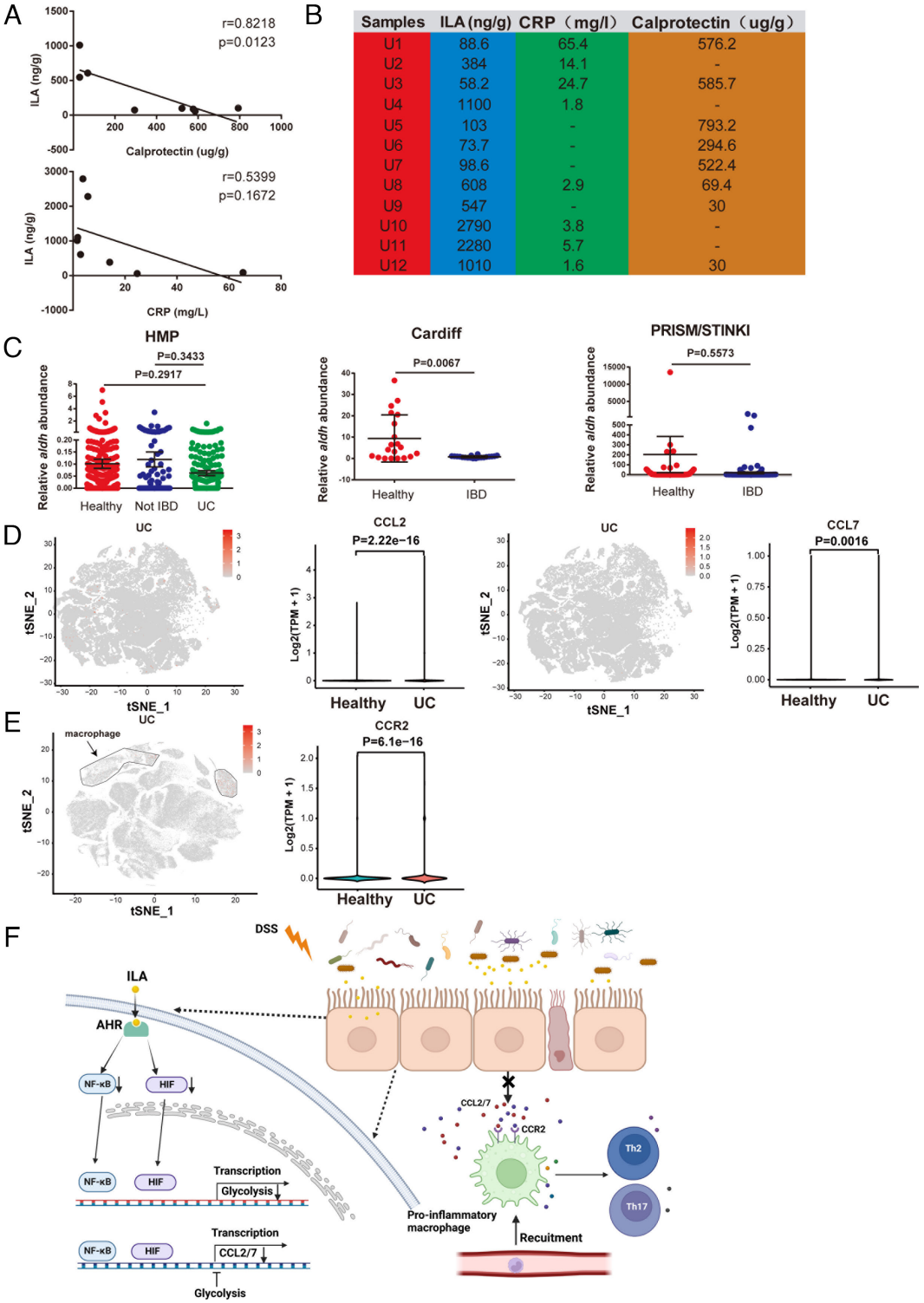

Fig. 7. The CCL2/7-CCR2 axis and ILA content are associated with IBD progression. (*A*) Pearson's correlation analysis of ILA levels and calprotectin or CRP (C-reactive protein) in the feces or blood from UC patients (Spearman's rank correlation coefficient, r = 0.8218/0.5399. Significance is assessed using linear regression, *P* = 0.0123/0.1672). (*B*) CRP, ILA, and calprotectin levels in the blood or stool of UC patients. (*C*) The *aldh* abundance of *Bifidobacterium* in available metagenomic data from IBD cohorts: HMP [n = 550 (Healthy) 140 (Not IBD) or 222 (UC)], Cardiff (n = 20), and PRISM/STINKI [n = 74 (CON) or 188 (IBD)]. (*D* and *E*) The scRNA-seq analysis of CCL2/7 and CCR2 in colon tissues of UC patients. (*D*) The expression of CCL2/7 in epithelial cells from colon biopsies of UC patients and healthy people. (*E*) The expression of CCR2 in macrophages from colon biopsies of UC patients and healthy people. (*F*) Graphical model illustrating the role of ILA in intestinal homeostasis. n = 8 (*A*). Data are the mean ± SEM. One-way ANOVA and unpaired Student's *t* test (*C*).

at the Department of Laboratory Animal Science and Technology, Tianjin Medical University. All male mice were used for experiments at 6 to 8 wk old. All experiments with mice were approved by the Animal Care and Use Committee, Tianjin Medical University (TMUaMEC 2023017).

Human Samples. To examine the role of gut microbiota affected by tinidazole in intestinal inflammation, we obtained stool samples of people treated with tinidazole or of healthy people from the School and Hospital of Stomatology in Tianjin Medical University. The average age of people treated with tinidazole was 23.1 (age range: 20–26; 3 males, 5 females) and of healthy donor was 22.4 (age range: 20–24; 2 males, 3 females). People treated with tinidazole were administered for three consecutive days at a dose of 1 g daily (*SI Appendix*, Table S2).

To validate the role of ILA in the development of IBD disease, we collected stool samples of patients with UC from Tianjin Medical University General Hospital, Tianjin, China. Informed consent was obtained from all subjects involved and the study with human samples was approved by the Ethics Committee of General Hospital, Tianjin Medical University, China (IRB2021-KY-318).

Bacterial Strains. Seven strains, namely *Lactococcus petauri*, *Klebsiella quasipneumoniae*, *Pediococcus acidilactici*, *Enterococcus lactis*, *Bifidobacterium pseudolongum*, *Ec-TMU*, and *K. singaporensis*, were isolated from the feces of people treated with tinidazole. Fecal pellets were homogenized in 1 mL of sterile phosphate-buffered saline solution containing 0.1% L-cysteine, then diluted serially and seeded on the Man Rogosa Sharpe agar (MRS) and BHI agar plates.

After being incubated in aerobic or anaerobic conditions at 37 °C for 24 to 72 h, single colonies with different morphological characteristics were picked up and transferred to the same medium for a further 2 or 3 d for purification and identification. *E. coli K12*, grown at 37 °C in Luria–Bertani (LB), was purchased from the Beijing Dingguo Biotechnology Development Center (Beijing, China).

Cells. Bone marrow–derived macrophages (BMDMs) were isolated from long bones of male C57BL/6J mice, and cultured in Dulbecco's modified Eagle's medium/F12 containing 10% heat-inactivated fetal bovine serum, penicillin (100 U/mL), streptomycin (100 μg/mL), and 10 ng/mL of murine M-CSF (315-02-50, Peprotech, Cranbury, NJ, USA) for 6 d. The human colorectal cancer cell line SW480 (ATCC ccl-228, RRID CVCL-0546) was obtained from ATCC. Cells were cultured with RPMI 1640 medium containing 10% bovine fetal serum in a cell culture incubator containing 5% CO2, humidified at 37 °C.

Antibiotic Treatment. To remove the intestinal commensal bacteria, mice were gavaged with a cocktail of antibiotics [AVMN, ampicillin (A610028-0025, 1 g/L), neomycin (A610366-0025, 1 g/L), metronidazole (A600633-0025, 1 g/L), and vancomycin (A600983-0001, 500 mg/L), SangonBiotech, Shanghai, China] in addition with AVMN-containing drinking water for 5 to 7 d. AVMN-containing water was renewed every 3 to 4 d to maintain efficacy.

DSS-Induced Acute Colitis Mouse Model. Acute colitis was induced in mice using DSS (0216011090, M.W. = 36,000–50,000 Da; MP Biomedicals, Solon, OH, USA). The mouse model to assess the anti-inflammatory properties of individual strains has been shown in Fig. 2*A*. Individual strains from the stool of mice were inoculated into 10 mL of sterile BHI broth containing 0.1% L-cysteine and cultured under anaerobic conditions for 24 h at 37 °C. After centrifugation (5,000 g for 5 min at 4 °C), bacterial liquid was resuspended in PBS at a concentration of 5×10^9 CFU/mL. After 5 d of AVMN and 1 d of water treatment, mice were gavaged with 200 μL liquid bacterial strains (10^9 CFU) once per day for 12 d, during which colitis was induced by 3.5% DSS and LPS (8 mg/kg body weight/day, L2880, Sigma-Aldrich, St. Louis, MO, USA).

The mouse model to explore the therapeutic effect of an individual strain on DSS-induced colitis without intestinal bacteria has been shown in Fig. 2*F*. After AVMN-cleaned intestinal bacteria, mice were treated with individual strain, 3.5% DSS, and LPS (8 mg/kg body weight/day) simultaneously for 6 d.

The mouse model to evaluate the prophylactic efficacy of an individual strain on DSS-induced colitis in the presence of intestinal bacteria has been shown in *SI Appendix*, Fig. S2*A*. After 7 d of pretreatment with strains, mice were gavaged with strains for 7 d while receiving 2.5% DSS in drinking water.

The mouse model to study the therapeutic efficacy of individual strains on DSS-induced colitis in the presence of intestinal bacteria or without the presence of other bacteria has been shown in Fig. 2*K* and *SI Appendix*, Fig. S2*F*. Mice were treated with strain and 2.5% DSS simultaneously for 8 d.

The mouse model to evaluate whether Ec-TMU gavage is harmful in mice has been shown in *SI Appendix*, Fig. S2*K*. Mice were gavaged daily with 10^9 CFU of each strain for 5 d after 5 d of AVMN and 1 d of water treatment.

The mouse model to test the therapeutic efficacy of ILA (I157602, Aladdin, China) on DSS-induced colitis has been shown in Fig. 5*I*. After 2 d of 2.5% DSS administration, mice were daily gavaged with sterile water or 40 mg/kg ILA in addition to the DSS administration.

The mouse model to test the prophylactic effect of ILA on DSS-induced colitis has been shown in *SI Appendix*, Fig. S7*E*. After 5 d of ILA pretreatment, mice were given 2.5% DSS simultaneously with ILA administration for another 5 d.

Body weight losses were calculated relative to the baseline weight of the same mouse before DSS administration. The sum of the body weight loss, stool consistence score, and blood in the stool was calculated as the DAI score. Stool consistency scores were determined as follows: 0 = normal; 1 = mild soft stools; 2 = very soft stools; 3 = watery stools. Stool bleeding scores were determined as follows: 0 = normal; 1 = brown color; 2 = reddish color; 3 = bloody stool. Body weight loss scores were determined as follows: 0 (<2%), 1 (2–5%), 2 (5–10%), 3 (10–15%), and 4 (more than 15%). Body weight loss and DAI were scored daily during DSS-induced colitis. For histological analysis, a distal part of colon tissue was fixed in 4% paraformaldehyde and embedded in paraffin. Tissue slides were stained with hematoxylin and eosin, then imaged by a microscope (BX46, Olympus, Tokyo, Japan). Seven parameters were used to determine the extent of the inflammation: (A) extent of inflammation (0–4), (B) extent of crypt damage (0–4), (C) infiltration of neutrophils and lymphocytes (0–3), (D) submucosal edema (0–3), (E) loss of goblet cells (0–3), (F) reactive epithelial hyperplasia (0–3), and (G) crypt abscesses (0–2) (37, 38).

Immunofluorescence Analysis. Colon tissues frozen in OCT compound were cut into 5-μm sections. The sections were fixed in cold acetone for 10 min at 4 °C and blocked with 5% BSA for 1 h. Samples were then incubated at 4 °C overnight with the indicated primary antibodies: CCL2 (1:200, SA00006-8, Proteintech) and Epcam (1:200, 21050-1-AP, Proteintech). Samples were washed with PBS and incubated for 1 h with an Alexa Fluor 488-labeled second antibody (1:400, SA00013-2, Proteintech) or an Alexa Fluor 594-labeled second antibody (1:400, SA00013-4, Proteintech). Nuclei were stained with DAPI. Images were captured by a confocal fluorescence microscope (Leica TCS-SP8, Leica Microsystems).

To test the effect of the supernatant, SW480 cells were simultaneously stimulated with bacterial culture supernatant (750 μL, <3 kDa) and LPS (10 μg/mL) for 3 h. To explore the role of ILA, SW480 cells were incubated with LPS (6 μg/mL) in addition with ILA (200 μM) or DMSO for 6 h, then fixed using 4% paraformaldehyde for 15 min following permeabilization with 0.25% Triton X-100 for 10 min. After being blocked in 5% normal goat serum for 1 h, the cells were incubated overnight with primary antibodies against CCL2 (1:200, Proteintech) and CCL7 (1:200, Bioss), followed by a washing step and incubation with an Alexa Fluor 488-labeled second antibody and DAPI. The fluorescence of sections was detected using a confocal fluorescence microscope (Leica TCS-SP8, Leica Microsystems, Germany).

Immunohistochemistry. Before immunostaining, tissue sections were deparaffinized and rehydrated, and antigen retrieval was performed in citrate buffer (pH 6). The sections were then treated with 0.3% hydrogen peroxide to block endogenous peroxidase activity. After being washed in PBS, tissues were blocked with 5% normal goat serum for 1 h and stained with the following primary antibody overnight: Muc2 (1:1,000, Proteintech), Ki67 (1:50, Abcam, Cambridge, MA, USA), Lgr5 (1:400, Affinity Biosciences, Cincinnati, OH, USA), Caspase3 (1:2,000, Cell Signaling Technology, Danvers, MA, USA), Occluding (1:200, Abcam), CCL7 (1:200, Bioss), p-IκBα (1:200, Affinity Biosciences), HIF1α (1:100, Affinity Biosciences), or CYP1A1 (1:200, Proteintech). The sections were repeatedly washed with PBS and stained with horseradish peroxidase (HRP)-labeled secondary antibody (Zsbio, Beijing, China) for 30 min at room temperature. Bound antibodies were measured with diaminobenzidine chromogenic substrate (Zsbio). The sections were finally counterstained with hematoxylin, dehydrated, and mounted. Tissues were examined and imaged using an Olympus BX46 microscope. The intensity of the staining was analyzed by the software Image Pro Plus.

ILA Concentration Measurement. The fraction of BHI, *Ec*-TMU, *Klebsiella singaporensis*, *K12* supernatant (< 3 kDa), and mice feces were collected and measured for ILA levels according to the manufacturer's instructions (Jiangsu Meimian Industrial Co., Ltd, MM-46497M2). Plates were read using the Thermo Multiskan Ascent Microplate Reader (Thermo Scientific).

ECAR. SW480 cells were pretreated with DMSO, AHR inhibitor (CH-223191, 10 μM), or HIF inhibitor (PX-478, 20 μM) for 4 h in 24-well Seahorse XFe-24 assay plates (Agilent, 102342-100), subsequently stimulating cells with DMSO or ILA (400 μM) for another 12 h. After 16 h, cells are stimulated with 6 μg/mL LPS for 6 h. For ECAR measurements, media were replaced with XF RPMI medium (pH 7.4) for 1 h at 37 °C. SW480 cells were treated with 10 μM glucose to determine the basal glycolytic capacity, with 1.5 μM oligomycin to determine the maximum glycolytic capacity, and with 50 μM 2-deoxy-D-glucose to determine glycolytic reserve. The results were assessed using Seahorse XFe-24 software (Agilent). Basal glycolysis was measured before the injection of oligomycin. The maximal glycolytic capacity is defined as the difference between subtracting the ECAR value after oligomycin injection and the ECAR in the absence of glucose. The glycolytic reserve was calculated as the average maximal ECAR values minus the ECAR values post glucose.

Macrophage Clearance In Vivo. The mouse model used to study the role of macrophages in the ILA treatment of DSS-induced colitis has been shown in *SI Appendix*, Fig. S8*A*. Mice were treated with CLP or PBS liposomes (CP-005-005, Target Technology, Beijing, China) to clear macrophages on days −1 and 4. After being injected with CLP or PBS liposomes on day −1, mice were given 2.5% DSS for 6 d. From day 2, mice were daily gavaged with sterile water or 40 mg/kg ILA and killed on day 6.

Measure of Lactate Concentrations in Isolated Colonic Epithelium. The colons extracted from male mice were washed with ice-cold PBS and cut into small pieces (≈1 mm). After incubating in ice-cold PBS containing 30 mM EDTA and 1.5 mM DTT for 30 min on ice, they were then suspended in PBS containing 30 mM EDTA at 37 °C for 10 min. Then, samples were shaken gently for 5 min to release epithelium from underlying muscular tissue, followed by the removal of excess tissue. After being separated by centrifugation (500 g, 5 min, 4 °C), the cells were washed twice with PBS and used for lactate quantification.

Lactate was measured according to the manufacturer's protocols (Sigma-Aldrich). Colonocytes were resuspended in 4 volumes of lactate assay buffer, mixed well, and centrifuged at 13,000 g for 10 min. Samples were deproteinized with 10-kD MWCO membranes (Merck Millipore). Then, 46 μL lactate assay buffer, 2 μL lactate enzyme mix, and 2 μL lactate probe were added to each of the wells. Reactions were incubated shaking at room temperature for 30 min. Absorbance was measured at 570 nm on the Thermo Multiskan Ascent Microplate Reader (Thermo Scientific).

Analysis of ILA in Human Feces. First, 50 mg of each sample was weighted, and 500 μL of initial mobile phase was added; the samples were then ground with steel balls for 3 min and centrifuged (20,000 g, 15 min, 4 °C). For LC-MS/MS detection and analysis, 200 μL of supernatant was taken. The targeted compounds were separated and quantified using a Vanquish liquid chromatography system coupled to a Thermo Scientific TSQ Altis Triple Quadrupole Mass Spectrometer with an ESI interface. The chromatographic separation was performed on a Phenomenex Kinetex F5 (250 × 4.5 mm, 5 μm) column. Ammonium acetate aqueous solution (10 mmol/L) and methanol were used as mobile phases. The sample injection volume was 5 μL. The column temperature was maintained at 35 °C. Sample introduction and ionization were performed by LC-MS/MS (positive ion mode).

NCBI Datasets. For the analysis of *aldh* abundance in fecal microbiota, data obtained from NCBI (PRJNA43017, PRJNA275349, PRJNA306874, PRJEB7949, and PRJNA385949) were analyzed by Iotabiome Biotechnology Co,. Ltd.

scRNA-seq Analysis. We use the Broad Institute Single Cell portal (https://singlecell.broadinstitute.org/single_cell/study/SCP259/intra-and-inter-cellular-rewiring-of-the-human-colon-during-ulcerative-colitis) to analyze available Single-cell RNA sequencing (scRNA-seq) data from colon biopsies of patients with UC. CCL2/7 and CCR2 expression was analyzed by Majorbio Bio-Pharm Technology Co., Ltd. (Shanghai, China).

Statistical Analysis. Data were presented as the mean ± SEM. The statistical significance of the differences was tested using one-way ANOVA or two-way ANOVA. All operations are performed in commercially available software (GraphPad Prism 6, San Diego, CA). Fig. 7*F* was created using Biorender (https://www.biorender.com/).

Data, Materials, and Software Availability. All data needed to evaluate the conclusions in the paper are present in the paper and/or the *SI Appendix*. Raw data for bacterial sequence were deposited in the NCBI Sequence Read Archive (SRA) database under accession numbers PRJNA946039 (18) and PRJNA945177 (15), respectively. RNA-sequencing data have been deposited in NCBI under accession numbers PRJNA946043 (16) and PRJNA946045 (17).

ACKNOWLEDGMENTS. We thank Prof. Huining He from Tianjin Medical University for providing help with some experiments. This study was supported by grants from the National Natural Science Foundation of China Programs (32170186, 82173199, and 82200618) and Tianjin Science and Technology Commissioner Project (22JCZDJC00490).

1. A. C. Luissint, C. A. Parkos, A. Nusrat, Inflammation and the intestinal barrier: Leukocyte-epithelial cell interactions, cell junction remodeling, and mucosal repair. *Gastroenterology* **151**, 616–632 (2016).
2. W. Liang *et al.*, FAM3D is essential for colon homeostasis and host defense against inflammation associated carcinogenesis. *Nat. Commun.* **11**, 5912 (2020).
3. T. Farinholt, C. Dinh, A. Kuspa, Social amoebae establish a protective interface with their bacterial associates by lectin agglutination. *Sci. Adv.* **5**, eaav4367 (2019).
4. Y. R. Na, M. Stakenborg, S. H. Seok, G. Matteoli, Macrophages in intestinal inflammation and resolution: A potential therapeutic target in IBD. *Nat. Rev. Gastroenterol. Hepatol.* **16**, 531–543 (2019).
5. C. C. Bain *et al.*, Resident and pro-inflammatory macrophages in the colon represent alternative context-dependent fates of the same Ly6Chi monocyte precursors. *Mucosal Immunol.* **6**, 498–510 (2013).
6. P. B. Eckburg *et al.*, Diversity of the human intestinal microbial flora. *Science* **308**, 1635–1638 (2005).
7. N. Sugimura *et al.*, *Lactobacillus gallinarum* modulates the gut microbiota and produces anti-cancer metabolites to protect against colorectal tumourigenesis. *Gut* **71**, 2011–2021 (2021).
8. Q. Li *et al.*, *Enterobacter ludwigii* protects DSS-induced colitis through choline-mediated immune tolerance. *Cell Rep.* **40**, 111308 (2022).
9. A. Lavelle, H. Sokol, Gut microbiota-derived metabolites as key actors in inflammatory bowel disease. *Nat. Rev. Gastroenterol. Hepatol.* **17**, 223–237 (2020).
10. L. A. Zenewicz *et al.*, Innate and adaptive interleukin-22 protects mice from inflammatory bowel disease. *Immunity* **29**, 947–957 (2008).
11. J. Qiu *et al.*, The aryl hydrocarbon receptor regulates gut immunity through modulation of innate lymphoid cells. *Immunity* **36**, 92–104 (2012).
12. R. S. Pollenz, The mechanism of AH receptor protein down-regulation (degradation) and its impact on AH receptor-mediated gene regulation. *Chem. Biol. Interact.* **141**, 41–61 (2002).
13. T. Zelante *et al.*, Tryptophan catabolites from microbiota engage aryl hydrocarbon receptor and balance mucosal reactivity via interleukin-22. *Immunity* **39**, 372–385 (2013).
14. M. Wlodarska *et al.*, Indoleacrylic acid produced by commensal *Peptostreptococcus* species suppresses inflammation. *Cell Host. Microbe.* **22**, 25–37.e6 (2017).
15. K. Yu, The feces of ILA treated mice. NCBI Sequence Read Archive (SRA). https://www.ncbi.nlm.nih.gov/sra/PRJNA945177. Accessed 16 March 2023.
16. K. Yu, Normal Transcriptome of human intestinal epithelial cell line NCBI Sequence Read Archive (SRA). https://www.ncbi.nlm.nih.gov/sra/PRJNA946043. Accessed 18 March 2023.
17. K. Yu, Normal RNA-seq of human intestinal epithelial cells. NCBI Sequence Read Archive (SRA). https://www.ncbi.nlm.nih.gov/sra/PRJNA946045. Accessed 18 March 2023.
18. K. Yu, Normal 16s RNA sequencing of human feces. NCBI Sequence Read Archive (SRA). https://www.ncbi.nlm.nih.gov/sra/PRJNA946039. Accessed 18 March 2023.
19. M. F. Laursen *et al.*, *Bifidobacterium* species associated with breastfeeding produce aromatic lactic acids in the infant gut. *Nat. Microbiol.* **6**, 1367–1382 (2021).
20. J. R. Grainger, J. E. Konkel, T. Zangerle-Murray, T. N. Shaw, Macrophages in gastrointestinal homeostasis and inflammation. *Pflugers Arch.* **469**, 527–539 (2017).
21. K. Papamichael *et al.*, Role for therapeutic drug monitoring during induction therapy with TNF antagonists in IBD: Evolution in the definition and management of primary nonresponse. *Inflamm. Bowel. Dis.* **21**, 182–197 (2015).
22. J. Ehrchen *et al.*, Glucocorticoids induce differentiation of a specifically activated, anti-inflammatory subtype of human monocytes. *Blood* **109**, 1265–1274 (2007).
23. A. C. Vos *et al.*, Anti-tumor necrosis factor-alpha antibodies induce regulatory macrophages in an Fc region-dependent manner. *Gastroenterology* **140**, 221–230 (2011).
24. J. He *et al.*, Fbxw7 increases CCL2/7 in CX3CR1hi macrophages to promote intestinal inflammation. *J. Clin. Invest.* **129**, 3877–3893 (2019).
25. Y. Yang *et al.*, Cross-talk between the gut microbiota and monocyte-like macrophages mediates an inflammatory response to promote colitis-associated tumourigenesis. *Gut* **70**, 1495–1506 (2020).
26. H. J. Kim *et al.*, ROS-induced PADI2 downregulation accelerates cellular senescence via the stimulation of SASP production and NFkappaB activation. *Cell. Mol. Life Sci.* **79**, 155 (2022).
27. R. M. Rodrigues, Y. Guan, B. Gao, Targeting adipose tissue to tackle NASH: SPARCL1 as an emerging player. *J. Clin. Invest.* **131**, e153640 (2021).
28. M. Sugahara *et al.*, Prolyl hydroxylase domain inhibitor protects against metabolic disorders and associated kidney disease in obese type 2 diabetic mice. *J. Am. Soc. Nephrol.* **31**, 560–577 (2020).
29. K. Peter, M. Rehli, K. Singer, K. Renner-Sattler, M. Kreutz, Lactic acid delays the inflammatory response of human monocytes. *Biochem. Biophys. Res. Commun.* **457**, 412–418 (2015).
30. V. Z. Wall *et al.*, Smooth muscle glucose metabolism promotes monocyte recruitment and atherosclerosis in a mouse model of metabolic syndrome. *JCI Insight* **3**, e96544 (2018).
31. B. Stockinger, K. Shah, E. Wincent, AHR in the intestinal microenvironment: Safeguarding barrier function. *Nat. Rev. Gastroenterol. Hepatol.* **18**, 559–570 (2021).
32. A. M. Ehrlich *et al.*, Indole-3-lactic acid associated with *Bifidobacterium*-dominated microbiota significantly decreases inflammation in intestinal epithelial cells. *BMC Microbiol.* **20**, 357 (2020).
33. D. Meng *et al.*, Indole-3-lactic acid, a metabolite of tryptophan, secreted by *Bifidobacterium longum* subspecies infantis is anti-inflammatory in the immature intestine. *Pediatr Res.* **88**, 209–217 (2020).
34. W. Huang, K. Y. Cho, D. Meng, W. A. Walker, The impact of indole-3-lactic acid on immature intestinal innate immunity and development: A transcriptomic analysis. *Sci. Rep.* **11**, 8088 (2021).
35. J. X. Han *et al.*, Microbiota-derived tryptophan catabolites mediate the chemopreventive effects of statins on colorectal cancer. *Nat. Microbiol.* **8**, 919–933 (2023).
36. Q. Q. Zhang *et al.*, Lactobacillus plantarum-derived indole-3-lactic acid ameliorates colorectal tumorigenesis via epigenetic regulation of CD8(+) T cell immunity. *Cell Metab.* **35**, 943–960 (2023).
37. H. Sann, J. Erichsen, M. Hessmann, A. Pahl, A. Hoffmeyer, Efficacy of drugs used in the treatment of IBD and combinations thereof in acute DSS-induced colitis in mice. *Life Sci.* **92**, 708–718 (2013).
38. K. Kabashima *et al.*, The prostaglandin receptor EP4 suppresses colitis, mucosal damage and CD4 cell activation in the gut. *J. Clin. Invest.* **109**, 883–893 (2002).